Source of Oligocene to Pliocene sedimentary rocks in the Linxia basin in northeastern Tibet from Nd isotopes: Implications for tectonic forcing of climate

Carmala N. Garzione†
Department of Earth and Environmental Sciences, University of Rochester, Rochester, New York 14627, USA, and *Department of Geological Sciences and Cooperative Institute for Research in Environmental Science, University of Colorado, Boulder, Colorado 80309, USA*

Matt J. Ikari
Asish R. Basu
Department of Earth and Environmental Sciences, University of Rochester, Rochester, New York 14627, USA

ABSTRACT

We used Nd isotopes and trace element data to determine the provenance of sedimentary rocks in the Linxia basin, northeastern Tibet, whose Oligocene through Pliocene sedimentation history has been interpreted to reflect deposition in a flexural basin associated with contractional deformation along the northeastern margin of the Tibetan Plateau. Paleozoic–early Mesozoic metasedimentary source rocks from the Kunlun-Qaidam and Songpan-Ganzi terranes have ε_{Nd} values between –11.8 and –16.1, whereas Paleozoic and Mesozoic plutonic source rocks that intrude the metasedimentary rocks have more positive ε_{Nd} values between –3.6 and –11.2. Cretaceous sedimentary source rocks display ε_{Nd} values of –9.7 and –9.9 in the Maxian Shan, north of the Linxia basin, and –15.3 in the plateau margin south of the basin. With ε_{Nd} values that range between –8.4 and –10.4 before ca. 15 Ma, and –6.2 and –11.8 after ca. 14 Ma, sedimentary rocks of the Linxia basin are less negative than metasedimentary rocks, which are dominant source rocks within the margin of the Tibetan Plateau today. The relatively positive ε_{Nd} values of Linxia basin sedimentary rocks could reflect several possible sources, including (1) a mixture of plutonic and metasedimentary rocks within the northeastern margin of Tibet, (2) Cretaceous sedimentary rocks derived from the north, or (3) loess derived from central Asian deserts. A mass balance calculation indicates that plutonic rocks are not volumetrically significant enough to generate the ε_{Nd} values observed in Linxia basin sedimentary rocks through mixing of plutonic and metasedimentary sources.

Rare earth element patterns suggest that Cretaceous rocks were not a dominant source of sediment. The Nd isotopic composition and rare earth element pattern of Quaternary loess are similar to older deposits in the Linxia basin and reflect loess deposited elsewhere in the Loess plateau and the North Pacific (ε_{Nd} = –8.6 to –10.5). In addition, the modern Daxia River, which drains the margin of the plateau today, transports clay and silt with ε_{Nd} values of –10.5 to –10.8 despite the river's source in more negative metasedimentary rocks of the Kunlun-Qaidam and Songpan-Ganzi terranes, which indicates that the modern fine-grained sedimentary budget is dominated by recent loess deposits. Considering the slow sedimentation rates in the Linxia basin, it is likely that loess sources have contributed a significant volume of fine-grained sediment to this basin throughout its history. An increase in the range of ε_{Nd} values at ca. 14 Ma in the Linxia basin may reflect increased unroofing of the northeastern margin of Tibet, which slightly preceded a change in climate between ca. 13 and 12 Ma in the Linxia basin. A 1.5‰ increase in baseline $\delta^{18}O$ values of lacustrine carbonates has been interpreted as the result of reorganization of atmospheric circulation and an increase in aridity on the northeastern margin of the Tibetan Plateau, perhaps associated with the plateau having achieved an elevation sufficient to block moisture from the Indian Ocean and/or Pacific Ocean. Similar timing of exhumation and climate change suggests that northeastward and eastward propagation of the plateau margin was responsible for the middle Miocene climate change observed in the Linxia basin.

Keywords: Nd isotopes, sedimentary provenance, loess, Tibetan Plateau, paleoclimate, unroofing.

INTRODUCTION

The unroofing histories of the margins of the Tibetan Plateau provide insight into the timing and mechanisms of outward growth of the plateau. The timing of surface uplift of the northeastern margin of the Tibetan Plateau is poorly understood because of the paucity of age constraints on exhumation in this region. Cenozoic sedimentary basins along the northeastern margin of Tibet contain records of both the unroofing history of the margin of the plateau and the evolution of central Asian climate. Potential sources of sediment to these basins include metasedimentary, plutonic, and sedimentary rocks exposed in the margin of the Tibetan Plateau as well as loess derived from central Asian deserts. Through an understanding of both the unroofing and climate histories in northeastern Tibet, we assessed the impact of the growth of the plateau on the regional climate.

Two types of data have been used to address the timing of Cenozoic deformation along the margin of the Tibetan Plateau: (1) subsidence histories from the records of sedimentation (e.g., Bally et al., 1986; Métivier et al., 1998; Yin et al., 2002; Fang et al. 2003; Horton et al., 2004), and (2) exhumation histories from thermochronologic studies of mountain ranges in the margins of the plateau (e.g., Jolivet et al., 2001; Sobel et al., 2001; Kirby et al., 2002;

†E-mail: garzione@earth.rochester.edu.

GSA Bulletin; September/October 2005; v. 117; no. 9/10; p. 1156–1166; doi: 10.1130/B25743.1; 9 figures; 2 tables; Data Repository item 2005145.

Clark et al., 2005). The earliest Cenozoic activity on the northern margin of Tibet is recorded by apatite fission-track and $^{40}Ar/^{39}Ar$ cooling histories from rocks along the Altyn Tagh and Kunlun faults, which suggest increased rates of exhumation in late Eocene to Oligocene time (Mock et al., 1999; Jolivet et al., 2001; Sobel et al., 2001). These ages are consistent with other observations from the northwestern Qaidam basin, including growth strata observed in seismic data (Bally et al., 1986); isopach data that show thick Oligocene deposition (Wang and Coward, 1990); and facies, paleocurrent, and provenance information that suggests positive relief in the Altyn Tagh (Hanson, 1998). Despite these older ages for initial exhumation along the Altyn Tagh fault, Tertiary fault offsets determined from sedimentary provenance relationships from the central and eastern parts of the fault have been interpreted as indicating a younger initial strike-slip motion of late Oligocene to early Miocene age (Yue et al., 2001, 2004; Ritts et al., 2004).

A second phase of exhumation in northern Tibet records higher rates in Miocene to Quaternary time. Apatite fission-track ages, associated with strike-slip deformation along the Altyn Tagh fault, show a Miocene-Pliocene increase in exhumation rates in the Qilian Shan, Kunlun Shan, and Altyn Tagh (Jolivet et al., 2001; George et al., 2001). In the southern Qaidam basin, an increase in sediment accumulation rates in middle to late Miocene time is consistent with these observations and suggests that contractional deformation was occurring in the Kunlun Shan at this time (Métivier et al., 1998). A larger increase in sediment accumulation rates throughout the Qaidam basin at ca. 5.3 Ma, followed by an increase in sediment accumulation in the Hexi Corridor in the Quaternary (Métivier et al., 1998), suggests a northeastward progression of deformation in the Qilian Shan along the northern margin of Tibet (Meyer et al., 1998; Métivier et al., 1998). The timing of increased rates of exhumation and sedimentation in northern Tibet agrees with the $^{40}Ar/^{39}Ar$ and (U-Th)/He thermal histories on the eastern margin of the Tibetan Plateau, which indicate that exhumation rates increased between ca. 13 and 5 Ma (Kirby et al., 2002; Clark et al., 2005).

The unroofing history recorded by sediments in the Linxia basin provides a useful comparison with the sedimentation and exhumation histories of the northern and eastern margins of the Tibetan Plateau. By comparing ε_{Nd} values and trace element patterns of Linxia basin sedimentary rocks to source rocks in northeastern Tibet and loess derived from central Asian deserts, we examined the timing of unroofing of the northeastern margin of the plateau and the significance of loess as a source of fine-grained sediment to the basin.

GEOLOGIC SETTING

Linxia Basin

The Linxia basin lies at the northeastern margin of the Tibetan Plateau in the eastern Kunlun-Qaidam terrane, southwest of Lanzhou (Fig. 1). The basin is ~200 km long and ~75 km wide and is elongate parallel to the fold-and-thrust belt on the northeastern edge of the Tibetan Plateau. The basin is situated between two major left-lateral strike-slip faults, the Haiyuan fault to the northeast and the Kunlun fault to the southwest (Fig. 1A and B). Movement along these faults and along the Altyn Tagh fault to the northwest allows eastward transfer of material in India's northward path into Eurasia and accommodates some of the convergence between India and Eurasia. Shortening at bends and terminations in these strike-slip faults creates some of the minor mountain ranges between them (e.g., Burchfiel et al., 1989; Tapponnier et al., 1990; Zhang et al., 1990, 1991).

The Linxia basin has been interpreted as a flexural basin on the basis of its shape, orientation, stratigraphy, and subsidence history (Fang et al., 2003). The stratigraphic thickness varies from >1200 m proximal to the plateau to <200 m near the southwestern flank of the Maxian Shan (Fig. 1). Fluvial and lacustrine deposits dominate the Linxia basin fill and were deposited on Paleozoic granite where the base of stratigraphic sections can be observed (Fang et al., 2003). Younger loess deposits form a set of terraces along the Yellow River and Daxia River, which document the Pleistocene incision of the Linxia basin (Li et al., 1997a).

Magnetic polarity stratigraphy provides age constraints of 29 to 4.5 Ma for the Linxia basin fill in the Maogou section in the central part of the basin (Fang et al., 2003) (Fig. 2). The upper Wangjiashan and nearby Dongshan sections are dated between 11 and 1.76 Ma on the basis of magnetostratigraphy (Li et al., 1997b; Fang et al., 2003). The lower Wangjiashan section (pre–11 Ma) is correlated with the dated Maogou section on the basis of lithology (Fang et al., 2003). Discrepancies between fossil ages in other nearby sections and magnetostratigraphy have led vertebrate paleontologists to suggest that the magnetostratigraphic record of Fang et al. (2003) may contain an error as large as 8 m.y. in the Oligocene part of the section and a hiatus of 4 m.y. between 8 and 12 Ma (Deng et al., 2004). It is unclear whether these discrepancies result from incorrect magnetostratigraphic correlations, uncertainty in fossil ages, or time transgressive facies between the fossil localities and paleomagnetic sections. The 4 m.y. hiatus seems unlikely in the Maogou and Wangjiashan sections, given that this interval is represented by apparently continuous lacustrine deposition in both sections and that both yield similar magnetostratigraphic records. Yet we acknowledge that age constraints may contain errors of up to several million years resulting from uncertainties in the magnetostratigraphic and lithostratigraphic correlations.

Plateau Margin

Southwest of the Linxia basin, the northeastern margin of the Tibetan Plateau consists of rocks of the eastern Kunlun-Qaidam terrane and the Songpan-Ganzi complex (e.g., Yin and Harrison, 2000) (Fig. 1B). North of the suture, the Kunlun-Qaidam terrane consists of Devonian through Permian metasedimentary rocks and plutons of early Paleozoic and late Paleozoic–early Mesozoic age. Devonian quartzites and interbedded red and green phyllites were deposited in a terrestrial environment, which may have developed as a result of the collision between the eastern Kunlun-Qaidam terrane and the southern Qilian Shan terrane to the north (Hsu et al., 1995). Devonian to Early Carboniferous quartzites and schists are interbedded with metavolcanic rocks associated with granitic intrusions (Yin et al., 1988; Huang et al., 1996). In Middle to Late Carboniferous time, this region underwent widespread deposition of shallow marine carbonates (Qinghai BGMR, 1991). Along the southern margin of Kunlun-Qaidam, a succession of Late Carboniferous through Early Permian marine sediments and interbedded volcanics, several kilometers thick, accumulated during rifting (Pierce and Mei, 1988), which removed part of the southern Kunlun-Qaidam terrane to form the Songpan-Ganzi ocean basin in Early Permian time (Yin and Harrison, 2000). These units were later metamorphosed during the latest Permian through latest Triassic northward subduction of the Songpan-Ganzi oceanic crust, which formed the younger superimposed arc within the Kunlun-Qaidam terrane (Jiang et al., 1992; Zhang and Zheng, 1994). Sediments that were deposited in the Songpan-Ganzi ocean basin are interpreted as submarine fan deposits that were derived from the Qinling orogenic belt, which developed as a result of the Triassic collision of the North and South China blocks (Yin and Nie, 1993; Zhou and Graham, 1996). These units were intensely folded during the Middle Jurassic closure of the Songpan–Ganzi–Hoh Xil ocean basin (Nie et al., 1994; Zhou and Graham, 1996). On the northern edge of the Linxia basin, the Maxian Shan is characterized by Jurassic

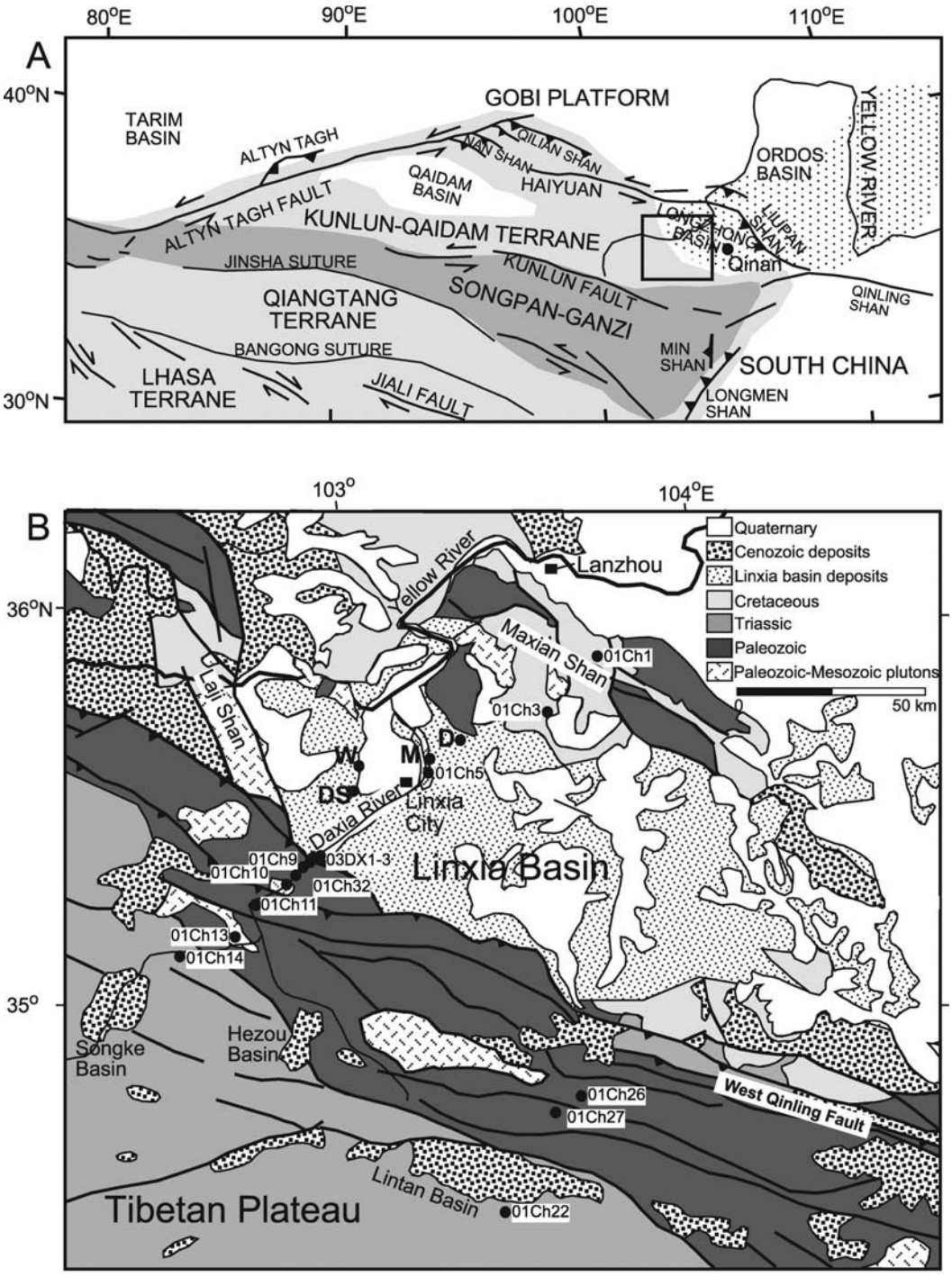

Figure 1. (A) Location of the study area (rectangle) relative to major tectonic elements of the Tibetan Plateau (simplified from Gaudemer et al., 1995). Medium gray region shows extent of the Tibetan Plateau, and stippled region shows extent of the Loess plateau. The darker gray region shows the extent of the Songpan-Ganzi accretionary wedge. (B) Simplified geologic map of the Linxia basin at the northeastern margin of the Tibetan Plateau (modified from Gansu Geologic Bureau, 1989), showing localities of studied sections in the Linxia basin. Thick lines are faults. Teeth are shown in the hanging walls of thrust faults. Black dots show locations of measured and sampled stratigraphic sections: W—Wangjiashan; M—Maogou; D—Dongxiang; DS—Dongshanding. Source rock samples are shown in Table 2.

to Paleocene deposits that have been broadly folded and overlie more intensely deformed Paleozoic rocks of the eastern Kunlun-Qaidam terrane (Gansu Geologic Bureau, 1989). Cretaceous sedimentary rocks that largely compose the Mesozoic cover are up to several kilometers thick and consist of fluvial conglomerate, sandstone, and mudstone. Quaternary loess deposits drape the region and are several tens to several hundreds of meters thick.

Nd ISOTOPE SYSTEMATICS

Linxia basin fill primarily consists of lacustrine mudstone and subordinate fluvial mudstone and sandstone. The lack of conglomeratic and coarse sandstone facies makes it difficult to determine the source of basin fill sediments using standard petrographic techniques (e.g., Dickinson and Suczek, 1979; Dickinson et al., 1983). Nd isotopes have been used in numerous previous studies to determine the provenance of fine-grained clastic sedimentary rocks (e.g., Michard et al., 1985; Frost and Winston, 1987; Gleason et al., 1995; Hemming et al., 1995; Garzione et al., 1997; Patchett et al., 1999; Robinson et al., 2001). Both Sm and Nd are rare earth elements (REE), which are all chemically similar and experience negligible fractionation during processes such as weathering, sediment transport, and deposition in fine-grained clastic

sedimentary rocks (Taylor and McLennan, 1985). Therefore, Nd isotopic compositions of Linxia basin mudstones and their possible sources can be compared to determine the source of fine-grained rocks in the Linxia basin.

SAMPLING AND EXPERIMENTAL METHODS

A total of 35 samples were analyzed for this study, including 19 Linxia basin samples, 13 source rock samples, and 3 modern clay-silt samples. The basin fill was sampled from three sections within the Linxia basin (Table 1; Fig. 1B). Source rock samples from the Kunlun-Qaidam and Songpan-Ganzi terranes were collected along two transects southwest of the basin (Table 2; Fig. 1B). Two Cretaceous samples were collected in the Maxian Shan, and one Cretaceous sample was collected in the plateau margin (Table 2; Fig. 1B). Source rock sample ages were assigned on the basis of existing maps (Gansu Geologic Bureau, 1989). Modern silt- and clay-sized sediment was sampled from the Daxia River where it exits the margin of the plateau and enters the Linxia basin (Table 2; Fig. 1B). Samples 03Dx1–03Dx3 were collected consecutively, with the next sample collected 1 km downstream of the previous locality.

Trace elements were analyzed with an inductively coupled–plasma mass spectrometer (ICP-MS PQ II+), and the Nd isotopic ratios were determined with a VG Sector thermal ionization mass spectrometer, both at the University of Rochester. For the ICP-MS analyses, 100 mg of powder was dissolved in Teflon bombs, diluted to 100 mL in a 5% HNO_3 solution with a 10 ppb internal standard of In, Cs, Re, and Bi. The trace element concentrations were obtained by using the known U.S. Geological Survey rock standards BCR-2 and BIR-2. The reported concentrations of the trace elements (Tables DR1 and DR2[1]) have 2–5% uncertainties on the basis of repeated measurements of SRM-278 (Obsidian-NIST) and BHVO (USGS-Basalt) rock standards that were analyzed as unknown samples.

Nd isotopes were measured with the chemical and mass spectrometric procedures established at the University of Rochester (Basu et al., 1990). Measured $^{143}Nd/^{144}Nd$ ratios were normalized to $^{146}Nd/^{144}Nd = 0.7219$. The La Jolla Nd standard analyzed during the course of this study yielded $^{143}Nd/^{144}Nd = 0.511856 \pm 24$ (2σ, $n = 5$). $\varepsilon_{Nd}(0)$ values were calculated using the present-day bulk earth value of $^{143}Nd/^{144}Nd$

[1]GSA Data Repository item 2005145, basin fill trace element data and source rock trace element data, is available on the Web at http://www.geosociety.org/pubs/ft2005.htm. Requests may also be sent to editing@geosociety.org.

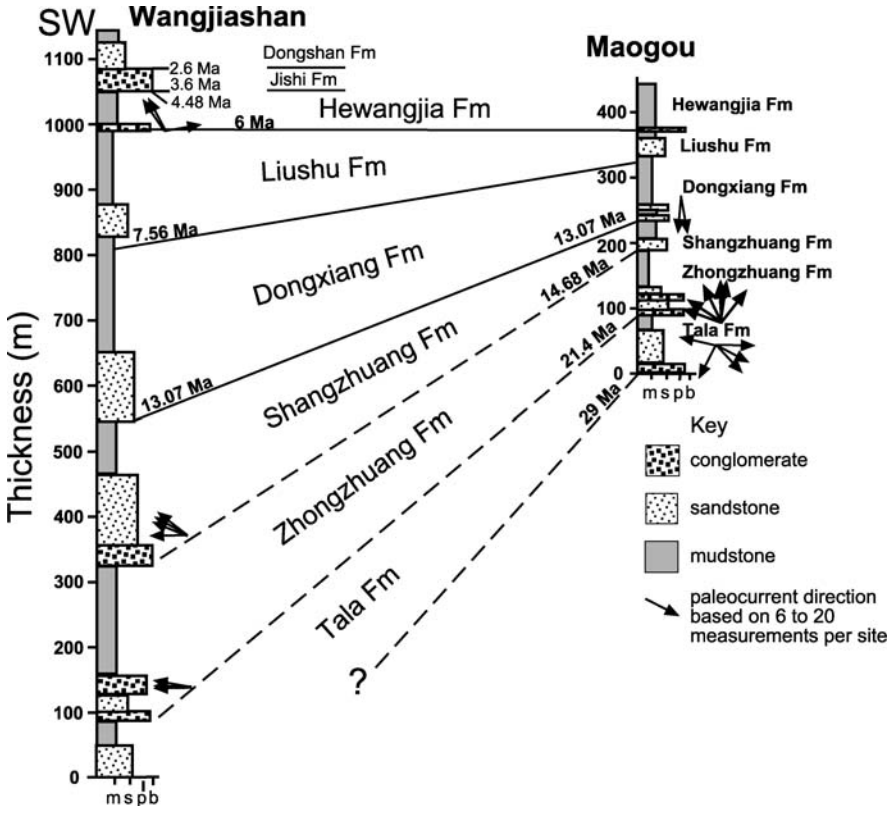

Figure 2. Stratigraphic correlation between two measured sections in Linxia basin. Solid lines are based on magnetostratigraphic correlation. Dashed lines are correlations based on lithofacies and mammalian fauna; m—mudstone; s—sandstone; p—pebble conglomerate; b—boulder conglomerate. Section locations are shown in Figure 1B.

TABLE 1. LINXIA BASIN Sm-Nd ISOTOPIC DATA

Sample	Formation	Description	$^{143}Nd/^{144}Nd$	±	$\varepsilon_{Nd}(0)$	Age (Ma)	$^{147}Sm/^{144}Nd$	$f_{Sm/Nd}$	T_{DM}
Maogou section									
01Mg3	Hewangjia	Brown mudstone	0.512320	24	–6.2	5.5	0.1309	–0.335	1.47
01Mg5	Liushu	Red mudstone	0.512171	29	–9.1	6.5	0.1286	–0.347	1.68
01Mg9	Dongxiang	Gray mudstone	0.512111	29	–10.3	8.8	0.1272	–0.354	1.76
01Mg16	Shangzhuang	Tan mudstone	0.512213	44	–8.3	13.7	0.1335	–0.321	1.71
01Mg17	Shangzhuang	Red mudstone	0.512148	27	–9.6	15.5	0.1283	–0.348	1.72
01Mg15	Zhongzhuang	Red mudstone	0.512176	22	–9.0	19.6	0.1281	–0.349	1.67
01Mg19	Tala	Tan mudstone	0.512205	41	–8.4	21.5	0.1281	–0.349	1.66
01Mg18	Tala	Red mudstone	0.512115	12	–10.2	28.5	0.1293	–0.343	1.79
Wangjiashan section									
01Dn1	Dongshan	Loess	0.512099	19	–10.5	2.5	0.1298	–0.340	1.83
01Wn51	Hewangjia	Tan mudstone	0.512121	29	–10.0	4.4	0.1431	–0.273	2.11
01Wn44	Liushu	Tan mudstone	0.512192	24	–8.7	6.6	0.1276	–0.351	1.63
01Wn39	Dongxiang	Red mudstone	0.512057	15	–11.3	8.4	0.1227	–0.376	1.76
01Wn36	Dongxiang	Red mudstone	0.512118	20	–10.1	11	0.1256	–0.362	1.72
01Wn27	Shangzhuang	Red mudstone	0.512225	34	–8.1	13.5	0.1251	–0.364	1.53
01Wn24	Shangzhuang	Tan mudstone	0.512031	24	–11.8	14.0	0.1281	–0.349	1.91
01Wn13	Zhongzhuang	Tan mudstone	0.512155	17	–9.4	15.0	0.1281	–0.349	1.70
01Wn10	Zhongzhuang	Red mudstone	0.512183	21	–8.9	18.5	0.1284	–0.348	1.66
01Wn16	Tala	Tan mudstone	0.512104	22	–10.4	22.0	0.1244	–0.368	1.72
01Wn1	Tala	Red mudstone	0.512119	10	–10.1	25.0	0.1301	–0.339	1.80

Notes: Ages were assigned based on magnetostratigraphy and lithostratigraphic correlation from Fang et al. (2003). $^{143}Nd/^{144}Nd$ ratios are normalized to $^{146}Nd/^{144}Nd = 0.7219$. Errors in the Nd isotopic ratios correspond to the 5th decimal place, reflect in-run precision, and are 2 standard errors of the mean in 40–100 ratios. ε_{Nd}, $f_{Sm/Nd}$, and T_{DM} were calculated using the model of DePaolo (1981). $\varepsilon_{Nd}(0) = \{[(^{143}Nd/^{144}Nd)_{sample}/(^{143}Nd/^{144}Nd)_{CHUR}] - 1\} \times 10^4$, where $(^{143}Nd/^{144}Nd)_{CHUR} = 0.512638$. (See text for further explanation.)

TABLE 2. SOURCE ROCK AND MODERN SEDIMENT Sm-Nd ISOTOPIC DATA

Sample	Description	$^{143}Nd/^{144}Nd$	±	$\varepsilon_{Nd}(0)$	$^{147}Sm/^{144}Nd$	$f_{Sm/Nd}$	T_{DM}
03Dx1	Daxia River clay-silt	0.512086	07	–10.8	0.1179	–0.401	1.52
03Dx2	Daxia River clay-silt	0.512096	06	–10.6	0.1348	–0.315	1.82
03Dx3	Daxia River clay-silt	0.512099	08	–10.5	0.1181	–0.399	1.50
01Ch6	Quaternary loess	0.512164	14	–9.2	0.1274	–0.353	1.67
01Ch11	Cretaceous mudstone	0.511850	17	–15.3	0.1228	–0.376	2.10
01Ch1	Cretaceous mudstone	0.512139	22	–9.7	-	-	-
01Ch3	Cretaceous mudstone	0.512133	38	–9.9	0.1417	–0.280	2.05
01Ch13	Mesozoic granodiorite	0.512062	14	–11.2	0.1148	–0.416	1.62
01Ch32	Mesozoic diorite	0.512334	10	–5.9	0.1265	–0.357	1.37
01Ch22	Upper Triassic slate	0.511711	29	–18.1	0.1076	–0.453	2.00
01Ch14	Triassic black slate	0.511879	29	–14.8	0.1330	–0.324	2.30
01Ch10	Permian black slate	0.511810	24	–16.2	0.1290	–0.345	2.31
01Ch27	Carboniferous phyllite	0.511941	27	–13.6	0.1317	–0.331	2.15
01Ch9	Carboniferous slate	0.512000	18	–12.4	0.1461	–0.258	2.46
01Ch26	Devonian phyllite	0.512032	15	–11.8	0.1295	–0.342	1.94
01Ch5	Paleozoic granite	0.512450	30	–3.7	0.1238	–0.371	1.14

Notes: Ages were assigned based on mapping of the Gansu Geologic Bureau (1989). $^{143}Nd/^{144}Nd$ ratios are normalized to $^{146}Nd/^{144}Nd = 0.7219$. Errors in the Nd isotopic ratios correspond to the 5th decimal place, reflect in-run precision, and are 2 standard errors of the mean in 40–100 ratios. ε_{Nd}, $f_{Sm/Nd}$, and T_{DM} were calculated using the model of DePaolo (1981). $\varepsilon_{Nd}(0) = \{[(^{143}Nd/^{144}Nd)_{sample}/(^{143}Nd/^{144}Nd)_{CHUR}] - 1\} \times 10^4$, where $(^{143}Nd/^{144}Nd)_{CHUR} = 0.512638$. (See text for further explanation.)

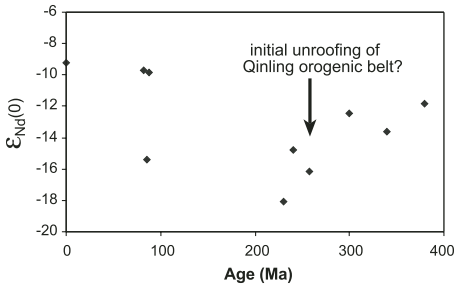

Figure 3. ε_{Nd} values of source rocks versus approximate age. Approximate timing of the collision of the North China and South China blocks is shown with an arrow. Subsequent erosion of older crustal sources in the Qinling orogenic belt provides an explanation for increasingly negative values in the Songpan-Ganzi complex.

= 0.512638, and the depleted mantle model ages (T_{DM}) of the sandstones were estimated by assuming a linear growth in the ε_{Nd} values of the depleted mantle from $\varepsilon_{Nd} = 0$ at 4.56 Ga to a present-day depleted mantle value of $\varepsilon_{Nd} = 10$ by using $^{147}Sm/^{144}Nd = 0.2136$. Enrichment factor $f_{Sm/Nd}$ was calculated as $f_{Sm/Nd} = [(^{147}Sm/^{144}Nd)_{sample}/(^{147}Sm/^{144}Nd)_{CHUR} - 1]$ where CHUR is chondritic uniform reservoir and $(^{147}Sm/^{144}Nd)_{CHUR} = 0.1967$. The three modern sediment samples from the Daxia River were analyzed for Nd isotopic compositions at the University of Arizona using methods described in Patchett and Ruiz (1987).

RESULTS

Source Rocks

The ε_{Nd} values observed in the different source rocks at the northeastern margin of the Tibetan Plateau provide a fingerprint of possible sources for Linxia basin sediment. Values of ε_{Nd} for metasedimentary source rocks between Devonian and Triassic age decrease over time from –11.8 to –18.0 (Fig. 3; Table 1). One Cretaceous mudstone from the margin of the plateau has a similar isotopic composition to metasedimentary rocks with $\varepsilon_{Nd} = –15.3$, whereas Cretaceous samples are significantly more positive in the Maxian Shan, with ε_{Nd} values of –9.7 and –9.9 (Fig. 3). The Paleozoic granitic basement on which Linxia strata were deposited has an ε_{Nd} value of –3.6, whereas two Mesozoic plutons within the Kunlun-Qaidam terrane have values of –11.2 and –5.9.

We also compared REE patterns for source and basin fill rocks with the post-Archean average Australian shale composite (PAAS) (Taylor and McLennan, 1985) to determine whether they reflect typical upper crustal patterns and to identify processes that may have fractionated the REE during sediment transport and deposition. With the exception of a Carboniferous slate sample (01Ch9), Devonian to Triassic metasedimentary rock samples are enriched in light REE and have negative Eu anomalies, displaying patterns and abundances similar to PAAS (Taylor and McLennan, 1985) (Fig. 4A; Table DR2; see footnote 1). Sample 01Ch9 has lower REE abundances and a flatter REE pattern than PAAS, with no Eu anomaly, suggesting that this rock had significant contributions from a mafic source. A Cretaceous mudstone (01Ch3) has a distinctive pattern, with a positive Ce anomaly and a minor negative Eu anomaly (Fig. 4A). The plutonic source rocks show a range of variability relative to typical upper continental crust with flatter light REE patterns and smaller to positive Eu anomalies (Fig. 4B), possibly reflecting contributions from mantle-derived sources.

Basin Fill

Mudstones from the Linxia basin yield ε_{Nd} values that range from –6.2 to –11.8 (Fig. 5; Table 1). For 29 to 15 Ma, ε_{Nd} values show a small range between –8.4 and –10.4. By 14 Ma, the scatter in the data increases, with values more positive and negative than the older sedimentary rocks in the basin.

REE patterns from both the Maogou section (Fig. 4C) and the Wangjiashan section (Fig. 4D) closely resemble PAAS in both shape as well as concentrations (~100 ppm) (Table DR1; see footnote 1). This suggests that processes such as heavy mineral sorting have not affected these rocks. A plot of $f_{Sm/Nd}$ versus ε_{Nd} (Fig. 6A) shows that Linxia basin mudstones plot in a mixing field bounded by plutonic and sedimentary-metasedimentary source rocks on either side. However, deposits between 29 and 15 Ma are tightly clustered about a Quaternary loess sample (see below) collected in the Linxia basin (Fig. 6B), whereas sedimentary rocks deposited between 14 and 2.5 Ma show much more scatter.

Modern Sediment and Quaternary Loess

Modern sediment samples from the Daxia River have ε_{Nd} values that range between –10.8 and –10.5. A Quaternary loess sample (01Ch6), collected from a terrace near the Maogou section, yielded an ε_{Nd} value of –9.2. In the plot of $f_{Sm/Nd}$ versus ε_{Nd}, both Daxia River muds and Quaternary loess plot within the range of ε_{Nd} values observed in Linxia basin sedimentary rocks (Fig. 6A). However, the mud samples collected from the Daxia River have slightly more negative ε_{Nd} values and display more scatter than the 29–15 Ma deposits in the Linxia basin (Figs. 5, 6A and B).

DISCUSSION

Trace Elements

REE patterns and concentrations of all Linxia basin mudstones are similar to those of PAAS, suggesting that they have not been

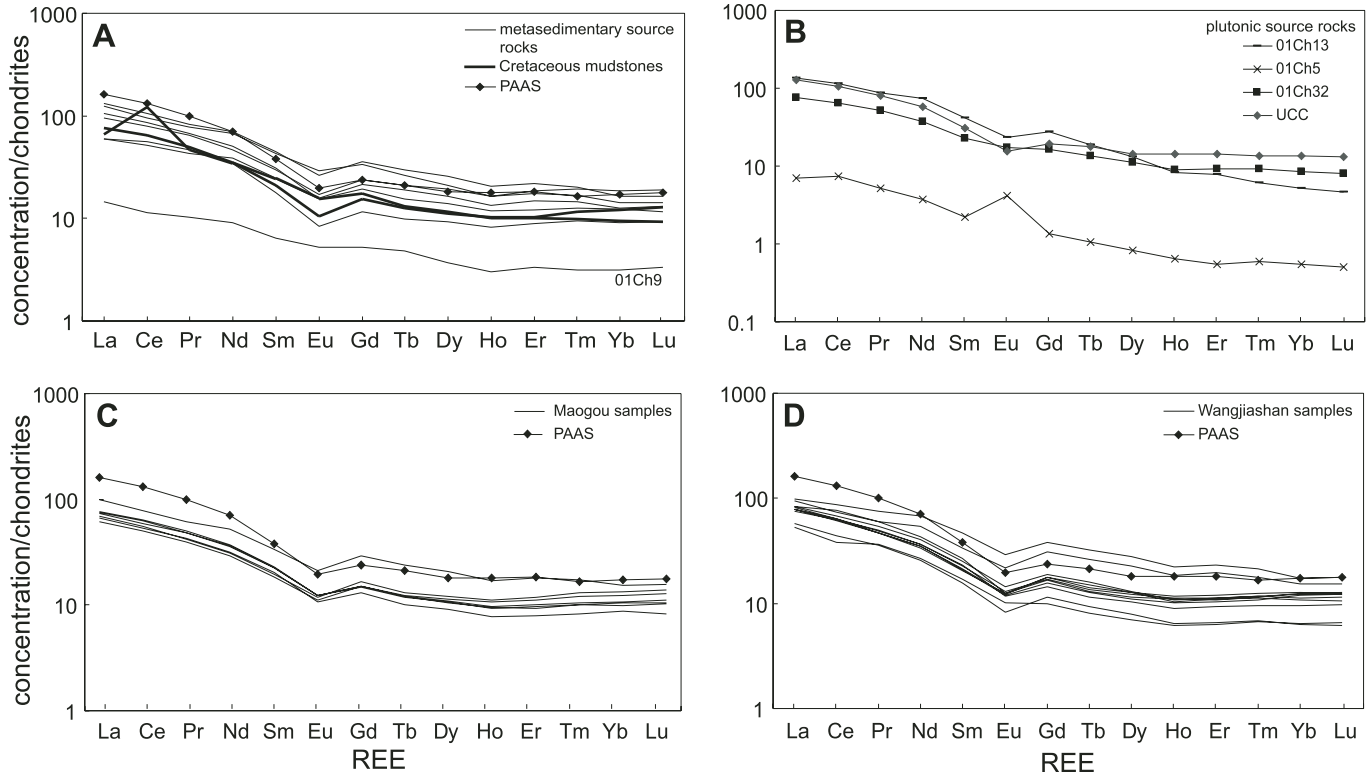

Figure 4. REE patterns for source rocks (A and B) and sedimentary rocks (C and D) within the Linxia basin. REE pattern for the post-Archean Australian shale composite (PAAS) is shown for comparison.

affected by factors that can upset relative REE concentrations. Most heavy minerals have a distinct REE pattern that differs from the pattern for typical continental crust (Taylor and McLennan, 1985). Therefore, a specific heavy mineral that is in greater abundance in the sedimentary rock can be identified by an increase in concentration of elements in the mineral as well as the mineral's influence on the REE pattern of the rock (McLennan et al., 1993). For example, zircon is enriched in heavy REE. Therefore, excess zircon would produce higher concentrations of Zr and higher Zr/Y ratios in sedimentary rocks along with heavy REE enrichment. The lack of positive correlation in the plot of Zr/Y versus Zr (Fig. 7), as well as the lack of heavy REE enrichment (Fig. 4C and D), suggests that no significant excess zircon is present in these samples.

The Gd/Yb ratio can be used to identify excess monazite in sedimentary rocks. Typical upper crustal rocks have Gd/Yb ratios that fall between 1.0 and 2.0 (McLennan, 1989). Monazite has very high REE abundances and a steep heavy REE pattern, which displays depletion in the heavy REE. Therefore, excess monazite should be associated with an increase in the Gd/Yb ratio relative to typical upper crustal rocks. In a plot of Gd versus Gd/Yb (Fig. 8) there is a slight positive correlation, with some Gd/Yb ratios higher than 2. This suggests that the heavy mineral monazite may be concentrated in some samples. However, the lack of very high Gd/Yb values and the similarity of the REE patterns and concentrations in comparison with typical continental crust indicate that not enough monazite is present to upset the relative abundances of REE in the samples.

A plot of Th/U versus Th can be used to evaluate the degree of weathering and mafic contributions to source rocks and sedimentary rocks in the Linxia basin (Fig. 9). Upper crustal Th/U values are generally between 3.5 and 4.0. High Th/U values are usually a sign of U loss during weathering under oxidizing conditions (McLennan et al., 1993). All but one Linxia basin sample (01Wn1) have values similar to typical upper crustal Th/U. This sample and three source rock samples (01Ch6, 01Ch11, and 01Ch26) have significantly higher Th/U values (>5) and therefore appear to have been weathered. Despite having undergone weathering, these samples display typical REE patterns in comparison with PAAS and upper continental crust, which suggests that their Nd isotopic compositions have not been affected by weathering. Two source rock samples (01Ch5 and 01Ch9) have lower

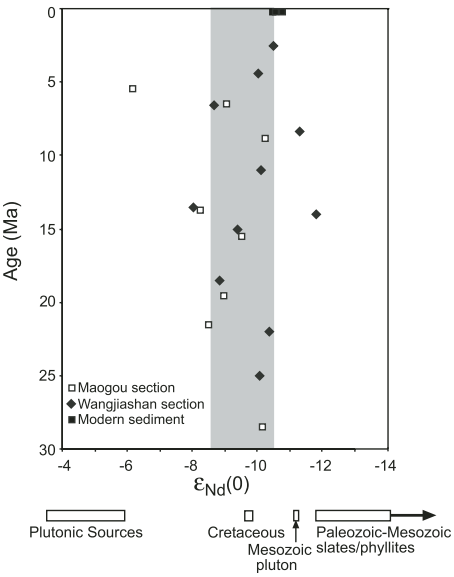

Figure 5. ε_{Nd} values of all Linxia basin samples versus magnetostratigraphic age: Wangjiashan samples (closed diamonds) and Maogou samples (open squares). The shaded area represents the range of ε_{Nd} values observed in the North Pacific dust record (Pettke et al., 2000).

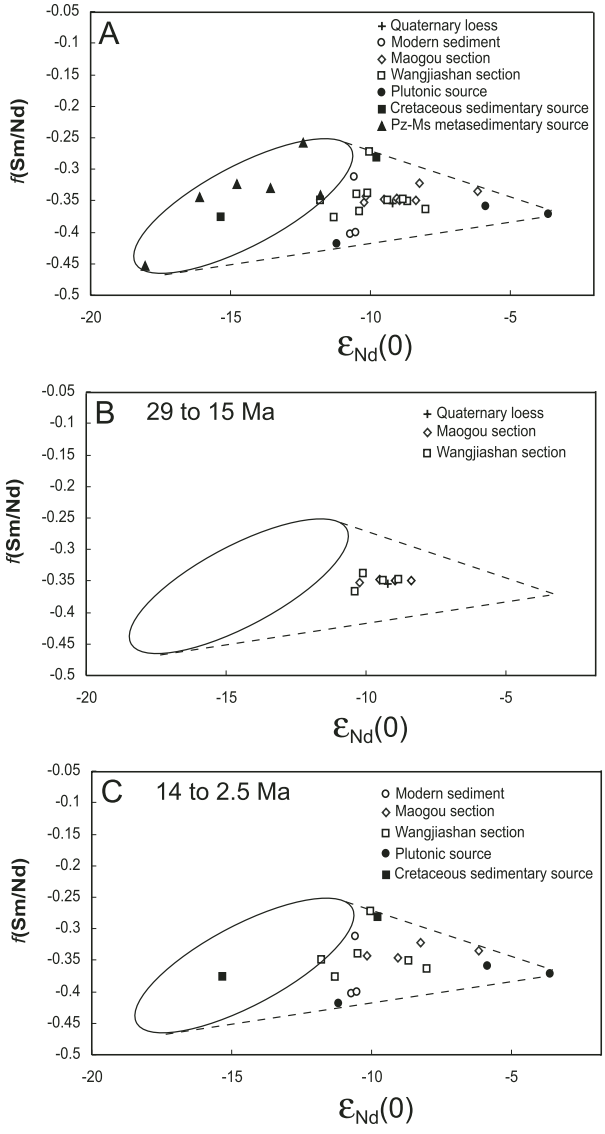

Figure 6. Plots of $f_{Sm/Nd}$ versus ε_{Nd}. Oval defines the field represented by metasedimentary source rocks in the Kunlun-Qaidam terrane and Songpan-Ganzi complex. Dashed lines define the mixing field represented by all other source rock samples (plutonic and Cretaceous sedimentary). (A) $f_{Sm/Nd}$ versus ε_{Nd} for all source rock and Linxia basin samples. Pz—Paleozoic; Ms—Mesozoic. (B) $f_{Sm/Nd}$ versus ε_{Nd} for all Linxia basin samples ≥15 Ma compared to Quaternary loess in Linxia basin. Tight clustering of Linxia basin sedimentary rocks and Quaternary loess supports the idea that early fine-grained sedimentation in the basin was dominated by loess. (C) $f_{Sm/Nd}$ versus ε_{Nd} for all Linxia basin samples ≤14 Ma compared to metasedimentary, plutonic, and Cretaceous sources, and modern sediment in the Daxia River. The scatter in Linxia basin sedimentary rocks reflects the range of values observed for source rocks in the margin of the plateau and suggests that significant contributions from these sources began by 14 Ma.

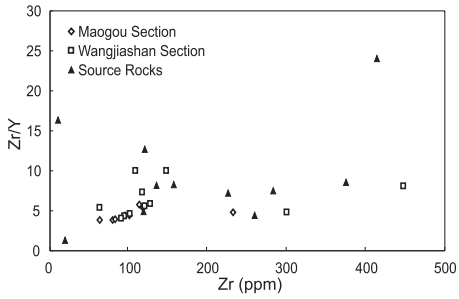

Figure 7. Plot of Zr/Y versus Zr for all samples. Lack of positive correlation indicates that the heavy mineral zircon is not significantly concentrated in these rocks.

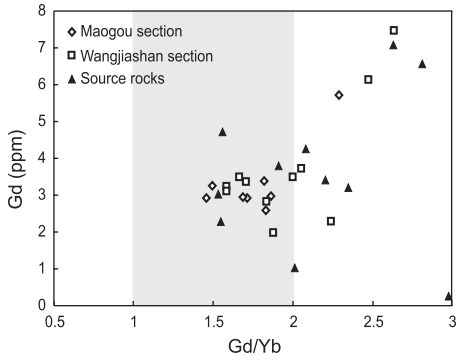

Figure 8. Plot of Gd versus Gd/Yb for all samples. Range of Gd/Yb in typical upper crustal rocks is shown with the gray band.

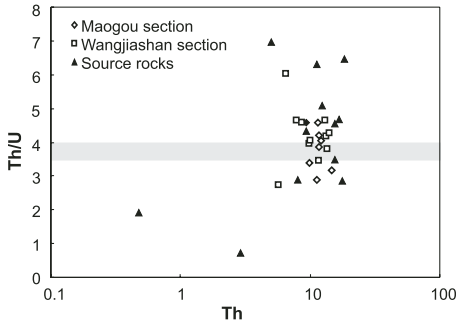

Figure 9. Plot of Th/U versus Th for all samples. The gray band shows the typical range of upper crustal Th/U.

Th/U ratios and Th concentrations, indicating contributions from mantle-derived sources (McLennan et al., 1993). Sample 01Ch5 is a Paleozoic granite with a relatively positive ε_{Nd} value of –3.6, a positive Eu anomaly, and low REE abundances (Fig. 4B), consistent with the interpretation that the lower Th/U reflects a mantle contribution. The only metasedimentary sample to have a low Th/U value (01Ch9) also displays a flatter REE pattern, no Eu anomaly, and lower REE abundances (Fig. 4A), all of which suggests a mantle-derived component in this rock. Despite evidence for significant mafic components in some of the source rocks at the northeastern margin of Tibet, Linxia basin sedimentary rocks show no evidence of a significant mafic provenance in either REE patterns or trace element concentrations.

Nd Isotopes

Metasedimentary units show decreasing ε_{Nd} values through time at the northeastern margin of the Tibetan Plateau (Fig. 3), which suggests contributions from an older crustal source beginning in Permian-Triassic time. Submarine fan deposits of the Songpan-Ganzi complex are interpreted to have been derived from the Qinling orogenic belt, which developed as a result of the Triassic collision of the North China and South China blocks (Yin and Nie, 1993; Zhou and Graham, 1996). The composition and U-Pb ages of single-grain detrital zircons of the Songpan-Ganzi strata suggest derivation predominantly from the North China block (Zhou and Graham, 1996; Bruguier et al., 1997). Therefore, the trend toward more negative ε_{Nd} values in the Triassic likely reflects the unroofing of older crustal source rocks in the North China block associated with the Qinling orogeny. Nd model ages (T_{DM}) between 2.0 and 2.3 Ga for the Songpan-Ganzi deposits are also consistent with a source region in the North China Block. The source for the less negative Cretaceous sedimentary rocks in the Maxian Shan is uncertain but may reflect the addition of more juvenile detritus from Jurassic volcanic rocks mapped within the Kunlun-Qaidam terrane in this region (Gansu Geologic Bureau, 1989) or mafic lithologies in basement rocks in ranges such as the Laji Shan.

The narrow range of ε_{Nd} values of –8.4 to –10.4 observed in sedimentary rocks of the Linxia basin between 29 and 15 Ma could have resulted from several different sources, including (1) a mixture of Devonian through Triassic metasedimentary sources and Paleozoic-Mesozoic plutonic sources within the northeastern margin of Tibet, (2) Cretaceous sedimentary rocks derived from the north, and (3) loess derived from central Asian deserts. To evaluate the likelihood of mixing between plutonic and metasedimentary sources, the necessary proportion of metasedimentary versus plutonic sources can be determined by taking the average isotopic compositions of metasedimentary and plutonic end members. If we average our samples, assuming a metasedimentary end member with an ε_{Nd} value of –14.4, and a plutonic end member of –6.9 with a similar concentration of REE, the mixture would have to consist of ~65% plutonic source rocks versus 35% metasedimentary source rocks. Considering that the rocks exposed on the northeastern margin of the plateau today consist of <10% plutonic rocks, this scenario seems highly unlikely.

The distribution of Cretaceous strata provides clues to whether they were a significant source of sediment to the Linxia basin. Oligo-Miocene Linxia basin deposits can be observed onlapping Cretaceous strata in the northeastern part of the basin. Toward the north, Cretaceous strata increase to a thickness of several kilometers, whereas in the central part of the basin the oldest deposits in the Maogou and Dongxiang sections (Fig. 1B) overlie Paleozoic granitic rocks. On the margin of the Tibetan Plateau, Cretaceous rocks are still preserved southeast of the Linxia basin, toward the west in the Laji Shan and in restricted outcrops south of the basin. Sparse paleoflow indicators in the Wangjiashan section show dominantly west-northwestward flow in the lower half of the section (Fig. 2), which suggests that these fluvial deposits represent an axial river system that flowed roughly parallel to the present-day plateau margin south of the Linxia basin. These sediment transport directions indicate that Cretaceous rocks southeast of the Linxia basin could have been a source of sediment to the basin, but these sources probably would have had relatively negative ε_{Nd} values, similar to sample 01Ch11 from the plateau margin. Sparse southward paleocurrent indicators from the Maogou section demonstrate that some sediment was derived from sources north of the basin. However, the REE pattern of a Cretaceous mudstone from the Maxian Shan (Fig. 4A) is distinctive from Linxia basin mudstones (Fig. 4C and D), which suggests that Cretaceous sources were not dominant. Considering the limited current distribution of Cretaceous strata and their highly variable ε_{Nd} values between –9.7 and –15.3, it seems unlikely that Cretaceous sources could have produced the relatively positive ε_{Nd} values in Linxia basin mudstones.

Several lines of evidence suggest that loess derived from central Asian deserts has provided a significant component of fine-grained sediment since the onset of deposition in the Linxia basin. The Nd isotopic composition of central Asian loess deposited on the Loess plateau over the past 800 k.y. ranges between –9.2 and –10.5 (Gallet et al., 1996; Jahn et al., 2001). These isotopic compositions compare well with the silicate fractions of pelagic sediment deposited in the North Pacific over the past 11 m.y. (ε_{Nd} = –8.6 to –10.5), which was presumably derived from central Asian loess (Pettke et al., 2000). The narrow range of ε_{Nd} values of –8.4 to –10.4 for Linxia basin mudstones deposited between 29 and 15 Ma in the Linxia basin is consistent with the isotopic composition from these long-term records of central Asian dust, suggesting that loess was the dominant source of fine-grained sediment to the Linxia basin since subsidence began in Oligocene time. In comparing the isotopic composition of Linxia basin mudstones with Quaternary loess deposited in the Linxia basin, a plot of $f_{(Sm/Nd)}$ versus ε_{Nd} shows a tight clustering of pre–15 Ma mudstones and a loess sample, indicative of similar REE patterns and isotopic compositions (Fig. 6B).

To test the plausibility of atmospheric dust dominating the fine-grained sediment budget in the Linxia basin, we compared sedimentation rates of pre–15 Ma deposits in the Linxia basin to loess sedimentation rates elsewhere east of the Tibetan Plateau. Loess deposition as early as 22 Ma in Qinan in the southwestern part of the Loess plateau (Fig. 1A) (Guo et al., 2002) has been documented, although widespread loess deposits in the Chinese Loess plateau before ca. 8 Ma (Sun et al., 1998; Ding et al., 1999; Qiang et al., 2001) have not been documented. In Qinan, the average dust accumulation rate between 22 and 6.2 Ma was 1.67 cm/k.y., whereas the average sedimentation rate for deposits older than 14.7 Ma in the central part of the Linxia basin (Maogou section) was 1.31 cm/k.y. Closer to the margin of the plateau in the Wangjiashan section, sedimentation rates were higher than at Qinan by a factor of 2 and averaged 3.58 cm/k.y. for rocks that are lithostratigraphically correlated with the Zhongzhuang Formation in the Maogou section (21.4–14.68 Ma). Given that Qinan is ~200 km east of the sections that we sampled in the Linxia basin, it is plausible that loess accumulation rates could have differed by a factor of 2. In addition, mudstone sedimentation in the Linxia basin occurred in lacustrine and fluvial depositional settings in a region that was undergoing tectonically driven subsidence (Fang et al., 2003). Therefore, greater accommodation space and higher sedimentation rates would be expected closer to the margin of the plateau, and locally deposited loess could have been eroded and transported by river systems feeding into the basin.

A further test of the ability of loess to dominate the fine-grained sedimentary budget in the Linxia basin would be to determine the isotopic composition of silt- and clay-sized sediment in modern rivers that drain the margin of the Tibetan Plateau. To characterize the composition of modern sediment being transported out of the margin of the plateau today, we analyzed the clay- and silt-sized fractions of sediment collected from the Daxia River, which flows northeastward into the Linxia basin (Fig. 1B), where it joins the Yellow River. A sample collected at the West Qinling fault at the southern margin of the basin yielded an ε_{Nd} value of –10.8. Two other samples, each collected 1 km downstream from the last, display increasing ε_{Nd} values of –10.6 and –10.5, perhaps reflecting an increase in loess influence heading northeastward into the basin. Assuming an average metasedimentary end member with an ε_{Nd} of –14.4, a loess end member with an ε_{Nd} of –9.5, and ignoring

the influence of plutonic rocks, which make up <10% of the source area, Daxia River muds would consist of 73% to 80% loess. Despite several kilometers of relief between the Linxia basin and the Tibetan Plateau, loess deposited within the Daxia drainage basin must consist of >~70% of the fine-grained component to produce the isotopic compositions observed at the Daxia River. Assuming less relief along the margin of the plateau early in Linxia basin history, and hence lower exhumation rates within metasedimentary rocks, it seems reasonable that loess could have dominated the fine-grained sedimentary budget.

By 14 Ma there was a much wider range of ε_{Nd} values in the Linxia basin, with ε_{Nd} values between –11.8 and –6.2 (Fig. 5). A plot of $f_{Sm/Nd}$ versus ε_{Nd} for sedimentary rocks ≤14 Ma (Fig. 6C) shows wider scatter than in pre–15 Ma rocks (Fig. 6B) and suggests additional contributions from metasedimentary and plutonic sources. We carried out one-tailed F tests for both ε_{Nd} and $f_{Sm/Nd}$ to examine the statistical significance of the difference in sample variance between pre–15 Ma and ≤14 Ma mudstones. The variance around the grand mean of each population (pre–15 Ma vs. ≤14 Ma) is estimated by taking the average sum of squared differences of each point from the population mean. The probability that the two distributions are not distinguishable is ~2% for ε_{Nd} and ~0.2% for $f_{Sm/Nd}$, which verifies a significant change in sample variance by ca. 14 Ma. More negative ε_{Nd} values observed after 14 Ma may reflect the unroofing of metasedimentary rocks of the Triassic Songpan-Ganzi complex and Paleozoic Kunlun-Qaidam terrane exposed today in the northeastern margin of Tibet, whereas sedimentary rocks with values more positive than loess may reflect contributions from plutonic sources. Despite additional contributions from older and younger sources after 14 Ma, most of the Linxia basin deposits continue to plot between –8 and –11, which suggests that loess must have continued to provide the dominant source of fine-grained sediment to the basin.

Implications for Plateau Unroofing and Climate Change

Trends in ε_{Nd} values in Linxia basin fill may reflect the history of unroofing of the northeastern margin of Tibet. Although loess most likely dominated the fine-grained sedimentary budget throughout the depositional history of the Linxia basin, an increase in the scatter of the Nd isotope data by 14 Ma, with both more negative and more positive values than loess, suggests an increase in contributions from Paleozoic and Mesozoic metasedimentary and plutonic sources at the northeastern margin of Tibet. This inference is supported by several other lines of evidence that indicate significant unroofing and climate change at approximately the same time. (U-Th)/He analysis of apatite from an elevation transect in the hanging wall of the West Qinling fault shows very slow exhumation from ca. 150 Ma to 45 Ma, a short period of more rapid exhumation of <1 km between 40 and 50 Ma, and followed by a deceleration in exhumation rate (M. Clark and K. Farley, 2004, personal commun.). The lowest sample in the elevation transect has an age of 9.9 Ma. Assuming a zero He age at the depth of the closure temperature at ~2.5 km beneath the modern topography, the exhumation rate must have increased in late Miocene time between ca. 14 and 6 Ma (M. Clark and K. Farley, 2004, personal commun.). In addition, detrital fission-track data from the Wangjiashan section show that by 14 Ma in the Linxia basin the youngest fission-track ages decrease significantly from ca. 74.3 to ca. 39 Ma (Zheng et al., 2003). This decrease in the lag time between fission-track age and the age of deposition indicates an acceleration of the rate of exhumation in the West Qinling Mountains by 14 Ma (Zheng et al., 2003). Fission-track, (U-Th)/He, and Nd isotope evidence for increased exhumation along the plateau margin by ca. 14 Ma agrees with the timing of a significant change in climate between ca. 13 and 12 Ma in the Linxia basin. Dettman et al. (2003) document a positive shift in the most negative $\delta^{18}O$ values of lacustrine carbonates in the Linxia basin that occurred between ca. 13 and 12 Ma. They attribute this positive shift to a change in the isotopic composition of meteoric water associated with reorganization of atmospheric circulation and an increase in aridity on the northeastern margin of the Tibetan Plateau and suggest that the plateau achieved an elevation sufficient to block moisture from the Indian Ocean and/or Pacific Ocean at this time.

The timing of increased exhumation of the West Qinling Mountains of ca. 14–12 Ma compares well with the initial timing of exhumation in eastern Tibet (Kirby et al., 2002; Clark et al., 2005) and northern Tibet (Jolivet et al., 2001; George et al., 2001) on the basis of thermochronologic studies and the timing of increased sediment accumulation in the Qaidam basin (Métivier et al., 1998). The similar timing of the onset of rapid exhumation along the northern, northeastern, and eastern margins of Tibet suggests that outward growth of the northeastern and eastern margins occurred as significant topographic relief developed along the northern margin. On the basis of Nd isotopes from the Linxia basin and other evidence for exhumation at this time, we suggest that northeastward and eastward growth of the plateau margin was responsible for the climate change observed in the Linxia basin.

Basin subsidence histories suggest that initial subsidence along the northern and northeastern margins of the plateau took place in Oligocene and possibly as early as middle Eocene time (Bally et al., 1986; Métivier et al., 1998; Yin et al., 2002; Fang, et al., 2003; Horton et al., 2004; Ritts et al., 2004). The gradual increase in subsidence rates observed in basins in northeastern Tibet (Fang et al., 2003; Horton et al., 2004) is consistent with flexural loading by contractional deformation as the dominant mechanism of subsidence and suggests that the load was smaller and/or more distal. Subsidence histories generally agree with apatite fission-track and $^{40}Ar/^{39}Ar$ cooling histories from rocks along the Altyn Tagh and Kunlun faults, which suggest increased rates of exhumation in late Eocene to Oligocene time (Mock et al., 1999; Jolivet et al., 2001; Sobel et al., 2001). Various forms of evidence have been used to infer high elevations in central and eastern Tibet by late Eocene time (Chung et al., 1998; Rowley and Currie, 2002). The earliest evidence for exhumation along the northeastern margin of Tibet indicates no more than ~1 km of exhumation, beginning at ca. 40–50 Ma on the southern margin of the Linxia basin (M. Clark and K. Farley, 2004, personal commun.), although widespread fine-grained sedimentation in the Linxia basin did not begin until ca. 29 Ma (Fang et al., 2003).

Previous studies have argued that the onset of loess deposition in the Loess plateau is related to uplift of the Tibetan Plateau by blocking moisture to the Asian interior and creating deserts capable of generating a large volume of loess (Guo et al., 2002; An et al., 2001). Other climate simulations that incorporate paleogeography have shown that the shrinking and isolation of the Paratethys seaway had equally drastic consequences for Asian climate by both increasing the amplitude of the seasonal cycle and thus strengthening the monsoon and decreasing the amount of precipitation in central Asia (Ramstein et al., 1997). The Qinan loess record, which has been dated to 22 Ma, has been used to infer that significant elevation had developed in southern Tibet by this time. Here we demonstrate that loess deposition began by ca. 29 Ma in the western part of the Loess plateau, ~10–20 m.y. after initial deformation of the margin of the plateau and the development of high elevation in the interior of the plateau. This age for initial loess deposition is more consistent with the early Oligocene timing of the final separation of the Paratethys seaway (Báldi, 1984; Rusu, 1985; Lorenz et al., 1993) and suggests that initial loess generation may have been

associated with land-sea distribution rather than Tibetan Plateau uplift.

CONCLUSIONS

Metasedimentary, plutonic, and sedimentary source rocks in the northeastern margin of the Tibetan plateau have distinctive Nd isotopic signatures through time, and trace element data indicate that Nd isotopic compositions are unaffected by factors such as weathering and heavy mineral sorting. Devonian and Carboniferous metasedimentary rocks have ε_{Nd} values ranging between –11.8 and –13.6, whereas Permian to Triassic metasedimentary rocks display increasingly negative ε_{Nd} values as low as –18, which suggests that these rocks had their source from older rocks in the active Qinling orogenic belt to the east. Paleozoic and Mesozoic plutonic rocks have more positive ε_{Nd} values of –11.2 to –3.6, which reflect contributions from the mantle. Cretaceous sedimentary rocks that cover the region have ε_{Nd} values that range between –9.7 and –15.3, and Quaternary loess and modern fine-grained sediment in the Linxia basin have ε_{Nd} values of –9.2 to –10.8.

The Nd isotopic compositions of Linxia basin sedimentary rocks provide insight into the dominant source of fine-grained siliciclastic sediment to the Linxia basin and the unroofing history of the northeastern margin of the Tibetan Plateau. Prior to 14 Ma, tightly constrained ε_{Nd} values between –8.8 and –10.4 suggest that loess derived from central Asian deserts was the dominant source of fine-grained sediment to the Linxia basin. Several lines of evidence support this inference, including (1) similarity in isotopic compositions between Linxia basin mudstones and ancient loess deposited in the Loess plateau and the North Pacific, (2) sufficiently low sedimentation rates in the Linxia basin to allow for loess to have made up a significant component of mudstone, and (3) predominance of loess in the silt- and clay-sized component of modern fine-grained sediment in the Daxia River, which drains older crustal sources at the northeastern margin of the plateau. By 14 Ma, more negative and more positive ε_{Nd} values ranging between –11.8 and –6.2 suggest an increase in the unroofing of Mesozoic and Paleozoic metasedimentary and plutonic sources in the northeastern margin of Tibet. This inference is supported by (U-Th)/He ages from plutonic rocks in the northeastern margin of the Tibetan Plateau and detrital fission-track ages from Linxia basin deposits that indicate both increased exhumation in the margin of the plateau at approximately the same time. Additional supporting evidence for increased tectonic activity in the margin of the plateau comes from a climate change event documented by a positive baseline shift in the oxygen isotopic composition of meteoric water in the Linxia basin between 13 and 12 Ma. This event is interpreted to represent a change in atmospheric circulation patterns and increased aridity in this region. Coeval exhumation along the northern, northeastern, and eastern margins of the plateau, associated with climate change observed in the Linxia basin, suggests that outward (eastward) growth of the plateau margin affected atmospheric circulation, which led to a drier climate along the northeastern margin of Tibet.

The older inception of loess deposition of ca. 29 Ma in the Loess plateau documented here calls into question the idea that initial loess generation in central Asian deserts is an indication of uplift of the Tibetan Plateau. The timing of initial deposition in the Linxia basin corresponds with the early Oligocene separation of the Paratethys seaway, which suggests that early loess deposition was related to land-sea distribution rather than uplift of the Tibetan Plateau.

ACKNOWLEDGMENTS

This paper is the result of a master's thesis by Matt Ikari. We would like to thank Fang Xiaomin, Song Chunhui, and Fan Majie for assistance in the field, and Aniki Saha, Ramananda Chakrabarti, and Clark Isachsen for their help with laboratory work. We are grateful to Peter Molnar, Marin Clark, and Jon Patchett for valuable discussions and reviews of an early version of this manuscript. We also thank David Barbeau, David Rea, and Matt Kohn for their constructive reviews.

REFERENCES CITED

An, Z., Kutzbach, J.E., Prell, W.L., and Porter, S.C., 2001, Evolution of Asian monsoons and phased uplift of the Himalaya-Tibetan plateau since Late Miocene times: Nature, v. 411, p. 62–66, doi: 10.1038/35075035.

Báldi, T., 1984, The terminal Eocene and Early Oligocene events in Hungary and the separation of an anoxic, cold Paratethys: Eclogae Geologocae Helvetiae, v. 77, p. 1–27.

Bally, A.W., Ryder, T., and Euster, H.P., 1986, Comments on the geology of the Qaidam basin, *in* Notes on sedimentary basins in China—Report of the American Sedimentary Basins Delegation to the People's Republic of China: U.S. Geological Survey Open-File Report 86-327, p. 42–62.

Basu, A.R., Sharma, M., and DeCelles, P.G., 1990, Nd, Sr-isotopic provenance and trace element geochemistry of Amazonian foreland basin fluvial sands, Bolivia and Peru: Implications for ensialic Andean Orogeny: Earth and Planetary Science Letters, v. 100, p. 1–17, doi: 10.1016/0012-821X(90)90172-T.

Bruguier, O., Lancelot, J.R., and Malavieille, J., 1997, U-Pb dating on single detrital zircon granites from the Triassic Songpan-Ganzi flysch (Central China); provenance and tectonic correlations: Earth and Planetary Science Letters, v. 152, p. 217–231, doi: 10.1016/S0012-821X(97)00138-6.

Burchfiel, B.C., Deng, Q., Molnar, P., Royden, L., Wang, Y., Zhang, P., and Zhang, W., 1989, Intracrustal detachment zones of continental deformation: Geology, v. 17, p. 748–752, doi: 10.1130/0091-7613(1989)017<0448:IDWZOC>2.3.CO;2.

Chung, S.-L., Lo, C.-H., Lee, T.-Y., Zhang, Y., Xie, Y., Li, X., Wang, K.-L., and Wang, P.-L., 1998, Diachronous uplift of the Tibetan plateau starting 40 Myr ago: Nature, v. 394, p. 769–773, doi: 10.1038/29511.

Clark, M.K., House, M.A., Royden, L.H., Whipple, K.X, Burchfiel, B.C., Zhang, X., and Tang, W., 2005, Late Cenozoic uplift of southeastern Tibet: Geology, v. 33, p. 525–528.

Deng, T., Wang, X., Ni, X., and Liu, L., 2004, Sequence of Cenozoic of the Linxia Basin, in Gansu, China: Acta Geologica Sinica, v. 78, p. 8–14.

DePaolo, D.J., 1981, Neodymium isotopes in the Colorado front range and crust-mantle evolution: Nature, v. 291, p. 193–196.

Dettman, D.L., Fang, X., Garzione, C.N., and Li, J., 2003, Uplift-driven climate change at 12 Ma: A long $\delta^{18}O$ record from the NE margin of the Tibetan plateau: Earth and Planetary Science Letters, v. 214, p. 267–277.

Dickinson, W.R., and Suczek, C.A., 1979, Plate tectonics and sandstone compositions: American Association of Petroleum Geologists Bulletin, v. 63, p. 2164–2182.

Dickinson, W.R., Beard, L.S., Brakenridge, G.R., Erjavec, J.L., Ferguson, R.C., Inman, K.F., Knepp, R.A., Lindberg, F.A., and Ryberg, P.T., 1983, Provenance of North American Phanerozoic sandstones in relation to tectonic setting: Geological Society of America Bulletin, v. 94, p. 222–235, doi: 10.1130/0016-7606(1983)94<222:PONAPS>2.0.CO;2.

Ding, Z.I., Xiong, S.P., Sun, J.M., Yang, S.L., Gu, Z.Y., and Liu, T.S., 1999, Pedostratigraphy and paleomagnetism of a ~7.0 Ma eolian loess–red clay sequence at Lingtai, Loess Plateau, north-central China and the implications for paleomonsoon evolution: Palaeogeography, Palaeoclimatology, Palaeoecology, v. 152, p. 49–66, doi: 10.1016/S0031-0182(99)00034-6.

Fang, X., Garzione, C.N., Van der Voo, R., Li, J., and Fan, M., 2003, Flexural subsidence by 29 Ma on the NE edge of Tibet from the magnetostratigraphy of Linxia basin, China: Earth and Planetary Science Letters, v. 210, p. 545–560.

Frost, C.D., and Winston, D., 1987, Nd isotope systematics of coarse- and fine-grained sediments: Examples from the Middle Proterozoic Belt-Purcell Supergroup: Journal of Geology, v. 95, p. 309–327.

Gallet, S., Jahn, B.M., and Torii, M., 1996, Geochemical characterization of the Luochan loess-paleosol sequence, China, and paleoclimatic implications: Chemical Geology, v. 133, p. 67–88, doi: 10.1016/S0009-2541(96)00070-8.

Gansu Bureau of Geology and Mineral Resources (GBGMR), 1989, Regional geology of Gansu Province (in Chinese with English summary): Beijing, Geologic Publishing House, 690 p.

Garzione, C.N., Patchett, P.J., Ross, G.M., and Nelson, J., 1997, Provenance of Paleozoic sedimentary rocks in the Canadian Cordilleran miogeocline: A Nd isotopic study: Canadian Journal of Earth Sciences, v. 34, p. 1603–1618.

Gaudemer, Y., Tapponier, P., Meyer, B., Peltzer, G., Guo, S., Chen, Z., Dai, H., and Cifuentes, I., 1995, Partitioning of crustal slip between linked, active faults in the eastern Qilian Shan, and evidence for a major seismic gap, the 'Tianzhu Gap', on the western Haiyuan fault, Gansu (China): Geophysical Journal International, v. 120, p. 599–645.

George, A.D., Marshallsea, S.J., Wyrwoll, K.H., Jie, C., and Yanchou, L., 2001, Miocene cooling in the northern Qilian Shan, northeastern margin of the Tibetan plateau, revealed by apatite fission-track and vitrinite-reflectance analysis: Geology, v. 29, p. 939–942, doi: 10.1130/0091-7613(2001)029<0939:MCITNQ>2.0.CO;2.

Gleason, J.D., Patchett, P.J., Dickinson, W.R., and Ruiz, J., 1995, Nd isotopic constraints on sediment sources of the Ouachita-Marathon fold belt: Geological Society of America Bulletin, v. 107, p. 1192–1210, doi: 10.1130/0016-7606(1995)107<1192:NICOSS>2.3.CO;2.

Guo, Z.T., Ruddiman, W.F., Hao, Q.Z., Wu, H.B., Qiao, Y.S., Zhu, R.X., Peng, S.Z., Wei, J.J., Yuan, B.Y., and Liu, T.S., 2002, Onset of Asian desertification by 22 Myr ago inferred from loess deposits in China: Nature, v. 416, p. 159–163, doi: 10.1038/416159a.

Hanson, A.D., 1998, Organic geochemistry and petroleum geology, tectonics, and basin analysis of southern

Tarim and northern Qaidam basins, northwest China [Ph.D. thesis]: Stanford, California, Stanford University, 388 p.

Hemming, S.R., McLennan, S.M., and Hanson, G.N., 1995, Geochemical and Nd/Pb isotopic evidence for the provenance of the early Proterozoic Virginia Formation, Minnesota: Implications for the tectonic setting of the Animikie basin: Journal of Geology, v. 103, p. 147–168.

Horton, B.K., Dupont-Nivet, G., Zhou, J., Waanders, G.L., Butler, R.F., and Wang, J., 2004, Mesozoic-Cenozoic evolution of the Xining-Minhe and Dangchang basins, northeastern Tibetan Plateau: Magnetostratigraphic and biostratigraphic results: Journal of Geophysical Research, v. 109, B04402, doi: 10.1029/2003JB002913.

Hsu, K.J., Pan, G., Şengör, A.M.C., Briegel, U., Chen, H., Chen, C., Harris, N., Hsu, P., Li, J., Lee, T., Li, Z.X., Lu, C., Powell, C., Wang, Q., and Winterer, E.L., 1995, Tectonic evolution of the Tibetan plateau: A working hypothesis based on the Archipelago model of orogenesis: International Geology Review, v. 37, p. 472–508.

Huang, H., Huang, Q., and Ma, Y., 1996, Geology of Qaidam Basin and its petroleum prediction: Beijing, Geological Publishing House, 257 p.

Jahn, B., Gallet, S., and Han, J., 2001, Geochemistry of the Xining, Xifeng and Jixian sections, Loess Plateau of China: Eolian dust provenance and paleosol evolution during the last 140 ka: Chemical Geology, v. 178, p. 71–94, doi: 10.1016/S0009-2541(00)00430-7.

Jiang, C., Yang, J., Feng, B., Zhu, Z., and Zhao, M., 1992, Opening-closing tectonics of Kunlun Mountains: Beijing, Geologic Publishing House, 224 p.

Jolivet, M., Brunel, M., Seward, D., Xu, Z., Yang, J., Roger, F., Tapponnier, P., Malavieille, J., Arnaud, N., and Wu, C., 2001, Mesozoic and Cenozoic tectonics of the northern edge of the Tibetan plateau: Fission-track constraints: Tectonophysics, v. 343, p. 111–134, doi: 10.1016/S0040-1951(01)00196-2.

Kirby, E., Reiners, P.W., Krol, M.A., Whipple, K.X, Hodges, K.V., Farley, K.A., Tang, W., and Chen, Z., 2002, Late Cenozoic evolution of the eastern margin of the Tibetan Plateau: Inferences from $^{40}Ar/^{39}Ar$ and (U-Th)/He thermochronology: Tectonics, v. 21, p. 1–20, doi: 10.1029/2000TC001246.

Li, J., Fang, X., Van der Voo, R., Zhu, J., MacNiocaill, C., Ono, Y., Pan, B., Zhong, W., Wang, J., Sasaki, T., Zhang, Y., Cao, J., Kang, S., and Wang, J., 1997a, Magnetostratigraphic dating of river terraces: Rapid and intermittent incision by the Yellow River of the northeastern margin of the Tibetan Plateau during the Quaternary: Journal of Geophysical Research, v. 102, p. 10,121–10,132, doi: 10.1029/97JB00275.

Li, J.J., Fang, X.M., Van der Voo, R., Zhu, J.J., Niocaill, C.M., Cao, J.X., Zhong, W., Chen, H.L., Wang, J., Wang, J.M., and Zhang, Y.C., 1997b, Late Cenozoic magnetostratigraphy (11–0 Ma) of the Dongshanding and Wangjiashan sections in the Longzhong Basin, Western China: Geologie en Mijnbouw, v. 76, p. 121–134.

Lorenz, C., Butterlin, J., Cavelier, C., Clermonte, J., Colchen, M., Dercourt, J., Guiraud, R., Montenat, C., Poisson, A., Ricou, L.-E., Sandulescu, M., Barrier, P., Bellion, Y., Benkhelil, J., Bonneau, J., Braud, J., Latreille, J., Marcoux, J., Mascle, G., 1993, Late Rupelian (30 to 28 Ma), *in* Dercourt, J., Ricou, L.E., and Vrielynck, B., eds., Atlas Tethys paleoenvironmental maps: Paris, Gauthier-Villars, p. 211–223.

McLennan, S.M., 1989, Rare earth elements in sedimentary rocks: Influence of provenance and sedimentary processes: Reviews in Mineralogy and Geochemistry, v. 21, p. 169–200.

McLennan, S.M., Hemming, S.R., McDaniel, D.K., and Hanson, G.N., 1993, Geochemical approaches to sedimentation, provenance, and tectonics, *in* Johnsson, M., and Basu, A., eds., Processes controlling the composition of clastic sediments: Geological Society of America Special Paper 284, p. 21–40.

Métivier, F., Gaudemer, Y., Tapponnier, P., and Meyer, B., 1998, Northeastward growth of the Tibet plateau deduced from balanced reconstruction of two depositional areas: The Qaidam and Hexi Corridor basins, China: Tectonics, v. 17, p. 823–842, doi: 10.1029/98TC02764.

Meyer, B., Tapponier, P., Bourjot, L., Métivier, F., Gaudemer, Y., Peltzer, G., Shunmin, G., and Zitai, C., 1998, Crustal thickening in Gansu-Qinghai, lithospheric mantle subduction, and oblique, strike-slip controlled growth of the Tibetan plateau: Geophysical Journal International, v. 135, p. 1–47, doi: 10.1046/j.1365-246X.1998.00567.x.

Michard, A., Gurriet, P., Soudant, M., and Albarede, F., 1985, Nd isotopes in Phanerozoic shales: External vs. internal aspects of crustal evolution: Geochimica et Cosmochimica Acta, v. 49, p. 601–610, doi: 10.1016/0016-7037(85)90051-1.

Mock, C., Arnaud, N.O., and Cantagrel, J.M., 1999, An early unroofing in northeastern Tibet? Constraints from $^{40}Ar/^{39}Ar$ thermochronology on granitoids from the eastern Kunlun range (Qianghai, NW China): Earth and Planetary Science Letters, v. 171, p. 107–122, doi: 10.1016/S0012-821X(99)00133-8.

Nie, S., Yin, A., Rowley, D., and Jin, Y., 1994, Exhumation of the Dabie Shan ultra–high pressure rocks and accumulation of the Songpan-Ganzi flysch sequence, central China: Geology, v. 22, p. 999–1002, doi: 10.1130/0091-7613(1994)022<0999:EOTDSU>2.3.CO;2.

Patchett, P.J., and Ruiz, J., 1987, Nd isotopic ages of crust formation and metamorphism in the Precambrian of eastern and southern Mexico: Contributions to Mineralogy and Petrology, v. 96, p. 523–528, doi: 10.1007/BF01166697.

Patchett, P.J., Roth, M.A., Canale, B.S., de Freitas, T.A., Harrison, J.C., Embry, A.F., and Ross, G.M., 1999, Nd isotopes, geochemistry, and constraints on sources of sediments in the Franklinian mobile belt, Arctic Canada: Geological Society of America Bulletin, v. 111, p. 578–589, doi: 10.1130/0016-7606(1999)111<0578:NICACO>2.3.CO;2.

Pettke, T., Halliday, A.N., Hall, C.M., and Rea, D.K., 2000, Dust production and deposition in Asia and the North Pacific Ocean over the past 12 Myr: Earth and Planetary Science Letters, v. 178, p. 397–413, doi: 10.1016/S0012-821X(00)00083-2.

Pierce, J.A., and Mei, H., 1988, Volcanic rocks of the 1985 Tibet geotraverse Lhasa to Golmud: Philosophical Transactions of the Royal Society of London, v. A327, p. 203–213.

Qiang, X., Li, Z., Powell, C.McA., and Zheng, H.B., 2001, Magnetostratigraphic record of the late Miocene onset of the East Asian Monsoon and Pliocene uplift of northern Tibet: Earth and Planetary Science Letters, v. 187, p. 83–93.

Qinghai BGMR (Qinghai Bureau of Geology and Mineral Resources), 1991, Regional Geology of the Qinghai Province: Beijing, Geological Publishing House, 662 p.

Ramstein, G., Fluteau, F., Besse, J., and Joussaume, S., 1997, Effect of orography, plate motion, and land-sea distribution on Eurasian climate change over the past 30 million years: Nature, v. 386, p. 788–795, doi: 10.1038/386788a0.

Ritts, B.D., Yue, Y., and Graham, S.A., 2004, Oligocene-Miocene tectonics and sedimentation along the Altyn Tagh Fault, Northern Tibetan Plateau: Analysis of the Xorkol, Subei, and Aksay Basins: Journal of Geology, v. 112, p. 207–229, doi: 10.1086/381658.

Robinson, D.M., DeCelles, P.G., Patchett, P.J., and Garzione, C.N., 2001, The kinematic evolution of the Nepalese Himalaya interpreted from Nd isotopes: Earth and Planetary Science Letters, v. 192, p. 507–521, doi: 10.1016/S0012-821X(01)00451-4.

Rowley, D.B., and Currie, B.S., 2002, Cenozoic paleoaltimetry and paleohypsometry of the Himalayas and Tibet plateau: Geological Society of America Abstracts with Programs, v. 34, no. 6, p. 472.

Rusu, A., 1985, Oligocene events in Transylvania (Roumania) and the first separation of Paratethys: Dari de Seama ale Sedintelor—Institutul de Geologie si Geofizica, v. 72–73, p. 207–223.

Sobel, E.R., Arnaud, N., Jolivet, M., Ritts, B.D., and Brunel, M., 2001, Jurassic to Cenozoic exhumation history of the Altyn Tagh Range, Northwest China, constrained by $^{40}Ar/^{39}Ar$ and apatite fission track thermochronology, *in* Hendrix, M.S., and Davis, G.A., eds., Paleozoic and Mesozoic Tectonic Evolution of Central and Eastern Asia: From Continental Assembly to Intracontinental Deformation: Geological Society of America Memoir 194, p. 247–267.

Sun, D., An, Z., Shaw, J., Bloemendal, J., and Sun, Y., 1998, Magnetostratigraphy and palaeoclimatic significance of late Tertiary aeolian sequences in the Chinese loess plateau: Geophysical Journal International, v. 134, p. 207–212.

Tapponnier, P., Lacassin, R., Leloup, P.H., Scharer, U., and Zhong, D., 1990, The Ailo Shan/Red River Metamorphic Belt: Tertiary left-lateral shear between Indochina and South China: Nature, v. 343, p. 431–437, doi: 10.1038/343431a0.

Taylor, S.R., and McLennan, S.M., 1985, The continental crust: Its composition and evolution: Cambridge, Massachusetts, Blackwell Science, 312 p.

Wang, Q., and Coward, M.P., 1990, The Chaidam basin (NW China): Formation and hydrocarbon potential: Journal of Petroleum Geology, v. 13, p. 93–112.

Yin, A., and Harrison, T.M., 2000, Geologic evolution of the Himalayan-Tibetan orogen: Annual Reviews of Earth and Planetary Sciences, v. 28, p. 211–280, doi: 10.1146/annurev.earth.28.1.211.

Yin, A., and Nie, S., 1993, An indentation model for North and South China collision and the development of the Tanlu and Honam fault systems, eastern Asia: Tectonics, v. 12, p. 801–813.

Yin, J., Xu, J., Liu, C., and Li, H., 1988, The Tibetan plateau: Regional stratigraphic context and previous work: Philosophical Transactions of the Royal Society of London, v. A327, p. 5–52.

Yin, A., Rumelhart, P.E., Butler, R., Cowgill, E., Harrison, T.M., Foster, D.A., Ingersoll, R.V., Zhang, Q., Zhou, X.Q., Wang, X.F., Hanson, A., and Raza, A., 2002, Tectonic history of the Altyn Tagh fault system in northern Tibet inferred from Cenozoic sedimentation: Geological Society of America Bulletin, v. 114, p. 1257–1295, doi: 10.1130/0016-7606(2002)114<1257:THOTAT>2.0.CO;2.

Yue, Y., Ritts, B.D., and Graham, S.A., 2001, Initiation and long-term slip history of the Altyn Tagh fault: International Geology Review, v. 43, p. 1087–1093.

Yue, Y., Ritts, B.D., Graham, S.A., Wooden, J.L., Gehrels, G.E., and Zhang, Z., 2004, Slowing extrusion tectonics: Lowered estimate of post–Early Miocene slip rate for the Altyn Tagh fault: Earth and Planetary Science Letters, v. 217, p. 111–122, doi: 10.1016/S0012-821X(03)00544-2.

Zhang, P., Burchfiel, C., Molnar, P., Zhang, W., Jiao, D., Deng, Q., Wang, Y., Royden, L., and Song, F., 1990, Late Cenozoic tectonic evolution of the Ningxia-Hui Autonomous Region, China: Geological Society of America Bulletin, v. 102, p. 1484–1498, doi: 10.1130/0016-7606(1990)102<1484:LCTEOT>2.3.CO;2.

Zhang, P., Burchfiel, C., Molnar, P., Zhang, W., Jiao, D., Deng, Q., Wang, Y., Royden, L., and Song, F., 1991, Amount and style of late Cenozoic deformation in the Liupan Shan area, Ningxia Autonomous Region, China: Tectonics, v. 10, p. 1111–1129.

Zhang, Y., and Zheng, J., 1994, Geologic overview in Kokshili, Qinghai and adjacent areas: Beijing, Seismological Publishing House, 177 p.

Zheng, D., Zhang, P., Wan, J., Li, C., and Cao, J., 2003, Late Cenozoic deformation subsequence in northeastern margin of Tibet: Science in China, v. 46, p. 266–275.

Zhou, D., and Graham, S.A., 1996, The Songpan-Ganzi complex of the western Qinling Shan as a Triassic remnant ocean basin, *in* Yin, A., and Harrison, T.M., eds., The tectonics of Asia: New York, Cambridge University Press, p. 281–299.

Manuscript Received by the Society 13 October 2004
Revised Manuscript Received 19 February 2005
Manuscript Accepted 10 April 2005

Printed in the USA